Preprint
UCRL-JC-143032

Thermodynamical Properties of ^{56}Fe

E. Tavukcu, J.A. Becker, L.A. Bernstein, P.E. Garrett, M. Guttormsen, G.E. Mitchell, J. Rekstad, A. Schiller, S. Siem, A. Voinov, W. Younes

This article was submitted to Frontiers of Nuclear Structure, Berkeley, CA, July 29 – August 2, 2002

August 30, 2002

U.S. Department of Energy

Lawrence Livermore National Laboratory

DISCLAIMER

Thermodynamical Properties of ^{56}Fe

E. Tavukcu*†, J.A. Becker†, L.A. Bernstein†, P.E. Garrett†, M. Guttormsen**, G.E. Mitchell*, J. Rekstad**, A. Schiller†**, S. Siem**, A. Voinov‡ and W. Younes†

*North Carolina State University, Raleigh, NC 27695
and Triangle Universities Nuclear Laboratory, Durham, NC 27708
†Lawrence Livermore National Laboratory, Livermore, CA 94551
**Department of Physics, University of Oslo, N-0316 Oslo, Norway
‡Frank Laboratory of Neutron Physics, Joint Institute of Nuclear Research, 141980 Dubna, Russia

Abstract.
Average nuclear level densities close to the nuclear binding energy in ^{56}Fe and ^{57}Fe are extracted from primary γ-ray spectra. Thermal properties of ^{56}Fe are studied within the statistical canonical ensemble. The experimental heat capacity is compared with the theoretical heat capacity calculated within the shell model Monte Carlo approach.

INTRODUCTION

Most experimental information on nuclear level densities comes from counting discrete levels at low excitations or from neutron-resonance spacing data at the neutron binding energy. Due to a rapid increase in the number of levels with increasing excitation energy, individual levels cannot be resolved experimentally. Therefore, it becomes impossible to measure the level density at high excitation energies, using common nuclear spectroscopy techniques. Recently, the Oslo Cyclotron group has developed a new method to extract average level densities up close to the neutron binding energy from primary γ rays [1]. This method also provides a simultaneous determination of the γ-ray strength function [1]. The method has been successfully applied to study several rare-earth nuclei where the level density is high [1, 2, 3, 4, 5]. In the present work we explore a lighter mass region, i.e. ^{56}Fe and ^{57}Fe isotopes which are close to a closed shell where strong single-particle effects are expected.

The nuclear level density is closely related to the thermodynamics of the nucleus. In fact, Bethe's pioneering work [6] to describe the level densities was based on calculating the entropy of the nucleus from the Fermi statistics. Recently, thermodynamic properties of several iron isotopes have been studied by Liu and Alhassid within the interacting shell model using the complete $(pf + 0g_{9/2})$-shell [7]. A signature of a pairing phase transition in the heat capacity is predicted by the calculations in the even-mass iron isotopes. The experimental and theoretical results will be compared.

EXPERIMENTAL DETAILS

The experiment was performed at the Oslo Cyclotron Laboratory with a 45-MeV ^{3}He beam on a self-supported ^{57}Fe target, which was 94.7% enriched and 3.38 mg/cm^2 thick. The (^{3}He,α) and (^{3}He,^{3}He') reactions in particular were studied. The reaction products are measured by the CACTUS multidetector array, which includes 8 Si(Li) particle telescopes and 28 NaI(Tl) detectors. The γ rays are measured in coincidence with the particles, which allows one to deduce the excitation energy of the final nucleus from reaction kinematics. The data were sorted into a two-dimensional excitation energy versus γ-ray energy matrix. Raw γ-ray spectra for 5-MeV excitations are shown at the top and bottom left panels in Fig. 1. Each excitation energy bin is 238-keV broad. The measured γ-ray spectra are then unfolded using the detector response functions in order to obtain the true γ-ray energy distribution [8] (see middle panel in Fig. 1). The primary γ-ray spectrum for each excitation energy bin is then extracted using a subtraction method developed by the Oslo Cyclotron group (see right panel in Fig. 1).

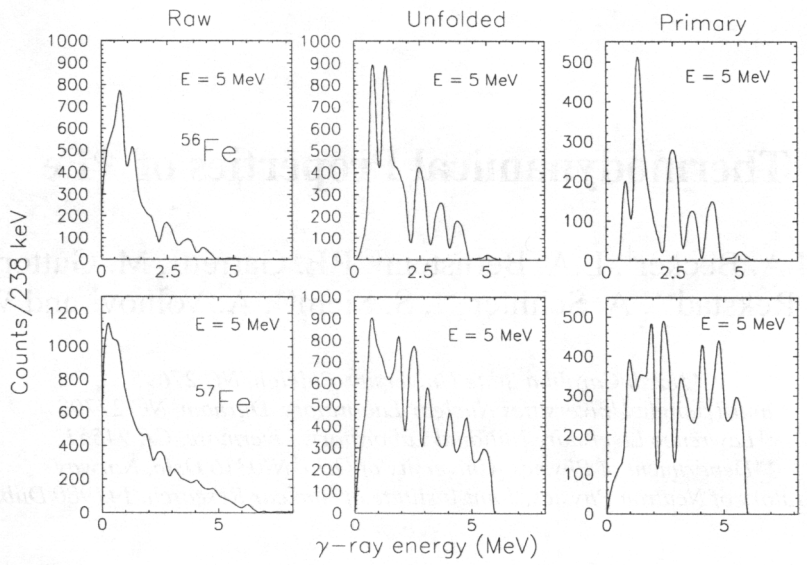

FIGURE 1. Raw (left), unfolded (middle), and primary (right) γ-ray spectra at 5 MeV of excitation energy for ^{56}Fe and ^{57}Fe.

The details of the subtraction method are given in Ref. [9]. The key assumption underlying the subtraction method is that the γ decay pattern from any excitation energy bin is independent of the population mechanism of the states within the bin, e.g. direct population by a nuclear reaction, or population in a nuclear reaction after one or several γ rays.

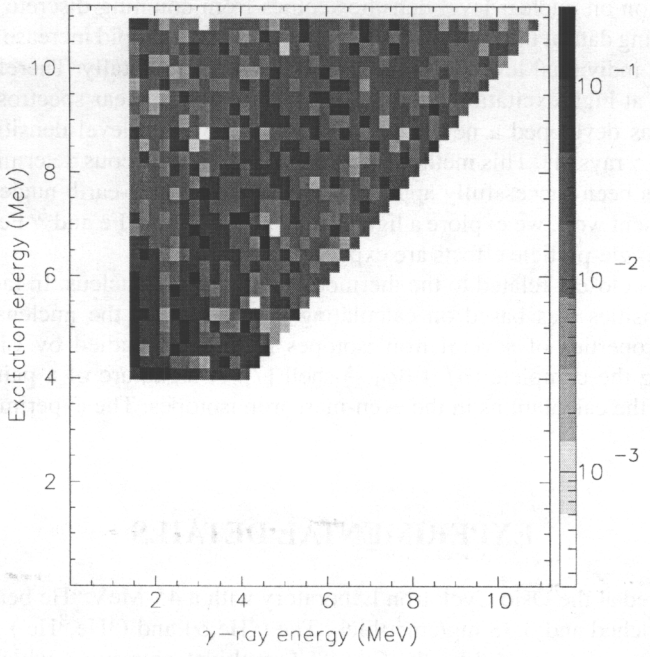

FIGURE 2. Experimental primary γ-ray matrix for ^{56}Fe.

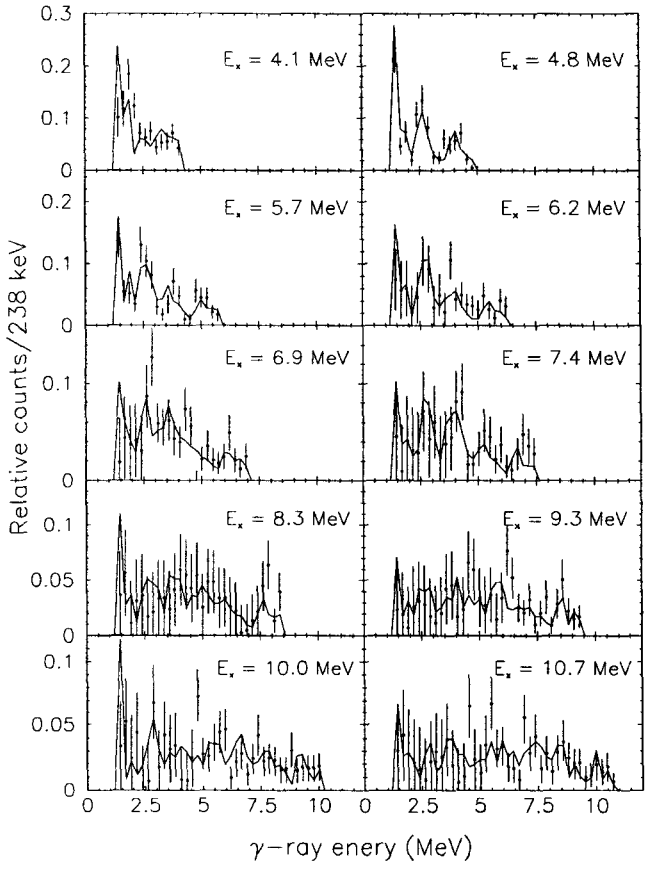

FIGURE 3. The experimental (data points) and calculated (solid line) primary γ-ray spectra for different excitation energies in ^{56}Fe.

METHOD

The method to extract the level density and γ-ray strength function simultaneously relies on the primary γ-ray spectra [1]. Once the primary γ-ray spectrum is normalized at each excitation energy, it represents γ-ray decay probability. Fig. 2 displays the normalized primary γ-ray matrix. Each square box represents one matrix element, and gives the probability of emitting a γ ray from the corresponding excitation energy. The matrix elements below E_x = 4 MeV of excitation energy are eliminated from the matrix since thermalization time might compete with the half life of the excited state, and therefore the reactions are likely to be more direct than compound. Furthermore, the matrix elements below E_γ = 1.5 MeV γ-ray energy are excluded due to ADC threshold walk, and bad timing properties of low-energy γ rays. There are also some problems associated with the subtraction method in obtaining the primary γ-ray spectra for low-energy γ rays. For example, the yrast γ rays are usually not properly subtracted, and any change in the spin population distribution between high and low excitations is not accounted for in the subtraction method.

The primary γ-ray matrix is factorized according to the Axel-Brink hypothesis [10, 11], which states that the probability of emitting a γ ray from an excited state is proportional to the γ-ray transmission coefficient and the level density at the final energy

$$P(E_x, E_\gamma) \propto F(E_\gamma)\rho(E_x - E_\gamma). \tag{1}$$

The final energy is given by the initial excitation energy minus the emitted γ-ray energy. Once the primary γ-ray matrix is factorized using the Axel-Brink hypothesis, the γ-ray transmission coefficient is a function only of the γ-ray energy, and the level density is a function only of the final excitation energy. This is the physical input in the method. If one writes out Eq. 1 for each primary γ-ray matrix element, it is clear that the vertical matrix elements depend on the function F at the same γ-ray energy. Similarly, the matrix elements along 45° will depend on the function ρ at the

same final excitation energy. Both F and ρ are unknown *a priori*. In order to find all of the F's and all of the ρ's, which will be referred to as one solution that describes the primary γ-ray matrix, we apply a least χ^2 method. In Fig. 3, both experimental and calculated primary γ-ray spectrum are plotted for several excitation-energy bins. The theoretical spectra, obtained by χ^2 minimization, reproduce the experimental spectra very well which justifies the assumption that the primary γ-ray spectrum can be factorized according to the Axel-Brink hypothesis.

It has been shown in Ref. [1] that one can find all other solutions with equal χ^2 by the transformation equations

$$\begin{aligned} \tilde{\rho}(E_x - E_\gamma) &= \rho(E_x - E_\gamma) A \exp(\alpha(E_x - E_\gamma)) \\ \tilde{F}(E_\gamma) &= F(E_\gamma) B \exp(\alpha E_\gamma), \end{aligned} \tag{2}$$

where A, B, and α are free parameters, F and ρ are the solutions obtained from the least χ^2 method, and $\tilde{F}$ and $\tilde{\rho}$ are the other solutions that can be obtained by giving different values to the free parameters A, B, and α. Now, using the transformation equations and the available known data, one can determine the most physical solution. We normalize the level density using the known discrete levels at low excitation, and the neutron-resonance spacing data at the binding energy. The normalization of the level density is performed by fitting the ratio $\tilde{\rho}/\rho$ with the transformation function $A\exp(\alpha(E_x - E_\gamma))$. Since there are no available neutron resonance data for the ^{56}Fe isotope, we normalize the level density in ^{56}Fe using information from the neighboring ^{57}Fe isotope. This is done as follows. A normalization factor is obtained by comparing the level density in ^{57}Fe from the neutron-resonance spacing data with the one calculated from the Fermi gas model using von Egidy's parameterization [12]. This factor is then applied to the calculated Fermi gas level density using von Egidy's parameterization at the neutron binding energy in ^{56}Fe in order to normalize the level density at high energies.

In the discussion that follows we concentrate on the level densities and some thermodynamical quantities that will be determined from the level density.

EXPERIMENTAL RESULTS

Level Densities in ^{56}Fe and ^{57}Fe

The normalized level densities for ^{56}Fe and ^{57}Fe are shown in Fig. 4. The empty triangle is the level density at the binding energy for the ^{57}Fe isotope, and is obtained from the neutron-resonance spacing data. The fact that the level density in ^{57}Fe is higher than the one in ^{56}Fe is a result of the unpaired neutron in ^{57}Fe. The level densities for both iron isotopes show a step-like behavior. First consider ^{56}Fe. The first bump corresponds to the first excited 2^+ state at 847 keV. The 4^+ state appears at around 2 MeV. Then one sees a plateau followed by a step at around 3 MeV. This step structure is a signature for the first pair breaking in ^{56}Fe, and can be compared with the predicted pairing gap parameter. We have calculated the pairing gap parameter using two different approaches, one is taken from Bohr and Mottelson [13], which uses a four-mass indicator, and the other is taken from Dobaczewski et al. [14], which uses a three-mass indicator. Ref. [14] has shown that three-mass indicator is able to separate pairing contribution and single-particle contribution in the odd-even mass staggering, and that the higher-order indicators mix the pairing and the single-particle contributions to the odd-even mass staggering. Since only the pairing contribution is of interest, the pairing gap parameters calculated from Ref. [14] are adopted in Fig. 4. The calculated pairing gap parameters are listed in Table 1 for both isotopes.

TABLE 1. The pairing gap parameters calculated from Dobaczewski et al. [14] and Bohr and Mottelson approaches [13].

	Δ_p(MeV) - ^{57}Fe	$\Delta_p + \Delta_n$(MeV) - ^{56}Fe
Dobaczewski et al.	0.82	2.27
Bohr and Mottelson	1.27	2.93

The first pair breaking is expected to be at $\Delta_p + \Delta_n$ in ^{56}Fe. The calculated $\Delta_p + \Delta_n$ is approximately 0.5 MeV below the energy of the first step at around 3 MeV. This is within reasonable agreement with the interpretation of the first pair breaking. Because one has to expend, in addition to the pairing energy, an energy in the order of ϵ, where ϵ is the single-particle energy, in order to break one pair and excite one of the nucleons into the lowest single-particle state. The step structure is washed out with increasing excitation energy.

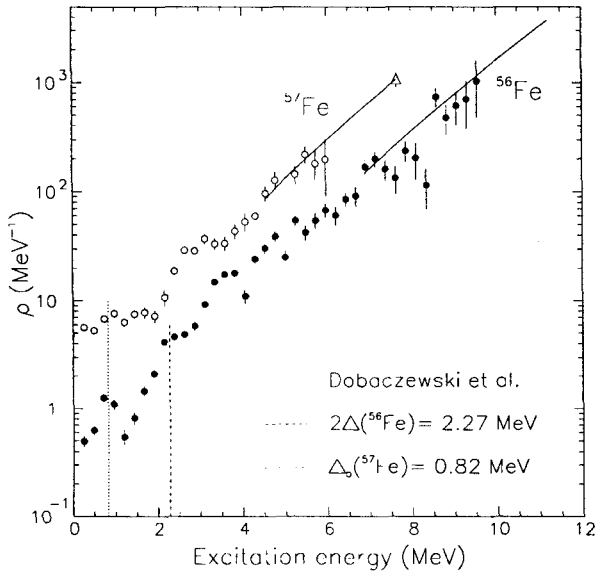

FIGURE 4. Level densities for the ^{56}Fe and ^{57}Fe isotopes.

The discrete structure at low excitation in ^{57}Fe is not as pronounced as in the ^{56}Fe case. Again this is because of the unpaired neutron in ^{57}Fe. It is commonly believed that neighboring odd-odd, odd-even, and even-even isotopes reveal the same level density if a proper shift is applied to the excitation energy. The step structure at around 2 MeV in ^{57}Fe would then correspond to the step observed at around 3 MeV in ^{56}Fe, taking into account an energy shift of about 1 MeV. Therefore, the steep increase at 2 MeV is interpreted as the first pair breaking, accordingly.

Thermodynamical Properties

Depending on the system under study, one can choose among different kinds of ensembles in order to derive thermodynamical quantities of the system. For small systems like a nucleus, it is difficult to chose an appropriate ensemble. The reason is the following. Although in general caloric curves derived within the microcanonical and canonical ensembles give the same result in the thermodynamic limit, the two caloric curves are different from each other for small systems. Furthermore, temperatures and heat capacities sometimes give negative values when derived within the microcanonical ensemble [3, 5]. On the other hand, the canonical ensemble averages too much over structural changes.

We derive thermodynamical properties of ^{56}Fe within the canonical ensemble. The canonical ensemble describes a system whose temperature is determined through contact with a heat reservoir. One defines the partition function in the canonical ensemble

$$Z(T) = \int_0^\infty \Omega(E) e^{-E/T} dE, \tag{3}$$

as the volume in phase space occupied by the canonical ensemble. $\Omega(E)$ is the multiplicity of states, and is proportional to the level density. The partition function is simply the Laplace transform of the multiplicity of states. From the basic principle of statistical mechanics, once the partition function is known, all thermodynamic properties can be determined.

It should be emphasized that we do not measure the temperature of the nucleus, but we measure instead the multiplicity of states, and then study how the nucleus behaves when it is connected to a heat bath. One can do this investigation with the probability density function, which is the probability of the system having energy E for a given temperature T, and is given by

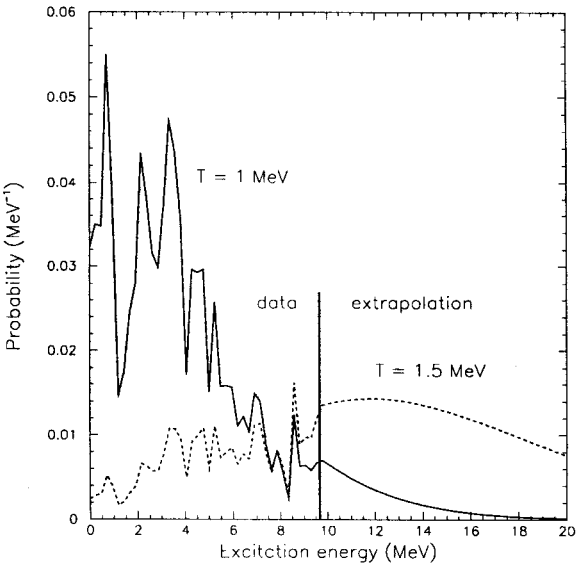

FIGURE 5. Probability density function for ^{56}Fe.

$$P(E) = \frac{\Omega(E)e^{-E/T}}{Z(T)}. \tag{4}$$

In Fig. 5 the probability density function is shown for temperatures T = 1 MeV and T = 1.5 MeV. Clearly, the probability distribution is mostly weighted by the experimental data for $T < 1$ MeV temperature. For increasing temperatures, the energy of the system increases; therefore, the probability density function depends more and more on the extrapolated level density. The integral in the partition function is defined from zero to infinity. However, our experimental level density goes up to around the binding energy. Therefore, the level density is extrapolated from about 10 MeV up to 150-MeV excitation energy using the Fermi gas model. The 150-MeV upper limit is sufficiently high for the integrand in Eq. 3 to vanish.

One should also notice in Fig. 5 that the energy of the system has a broad distribution for a given temperature, since we are dealing with small systems. Significant averaging over structural changes in the canonical ensemble is caused by the damping exponential in the calculation of the partition function. In the thermodynamic limit, or for large systems, the energy distribution becomes similar to a δ function from which the energy of the system can be defined quite well.

Alternatively, the relation between the energy and the temperature of the system can be studied using

$$E = T^2 \frac{\partial \ln Z(T)}{\partial T}, \tag{5}$$

which is called the caloric curve. The experimental caloric curve is shown in Fig. 6. Again one has to keep in mind that the caloric curve is only an approximation, since the energy of the system is quite uncertain for a given temperature (see Fig. 5).

Next, we would like to study the heat capacity in ^{56}Fe. The heat capacity is given by

$$C_V = \left(\frac{\partial E}{\partial T}\right)_V, \tag{6}$$

where E is the average energy of the system determined by the caloric curve (see Fig. 6). The heat capacity is a measure of the degrees of freedom of the nucleus. The heat capacity in several iron isotopes has been calculated by Liu and Alhassid using the shell model Monte Carlo (SMMC) approach with a complete $(pf + 0g_{9/2})$ shell [7]. In Fig. 7 the theoretical and experimental heat capacities are plotted. However, one should not directly compare the two,

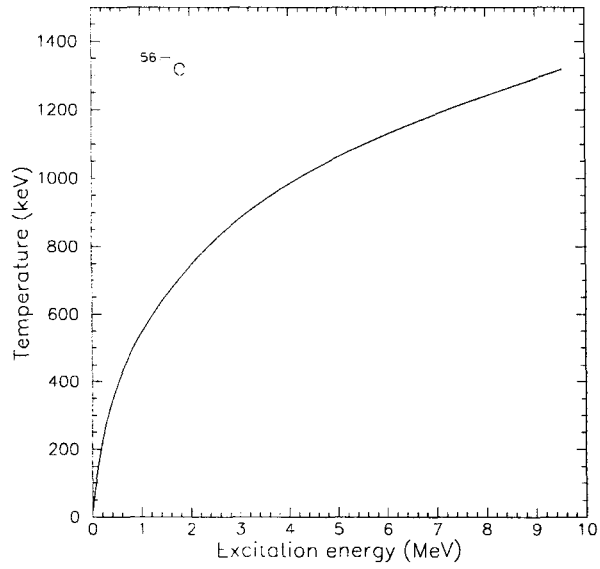

FIGURE 6. Caloric curve for ^{56}Fe.

since the theoretical calculations were performed using the state density, and the experimental heat capacity is obtained using the level density. The relation between the state and the level density is given by

$$W(E) = \sum_{J}(2J+1)\rho(E,J), \tag{7}$$

where $W(E)$ is the state density, which includes all of the magnetic substates. Clearly, the theoretical and the experimental heat capacities have local enhancement at different temperatures, 0.7 MeV and 1.3 MeV, respectively. The saturation above this enhancement in the model calculations is an artifact of the finite model space. Thus, as the temperature increases, the nucleons cannot be scattered across high energies since there are not enough single-particle levels to excite. Therefore, the heat capacity would eventually turn over and go to zero at high temperatures. This effect is known as the Schottky anomaly in the heat capacity [15].

The disagreement between the experimental and the theoretical heat capacities might be a result of the spin cut-off parameter. In order to deduce the density of levels of given angular momentum J at a given energy, one needs to know the spin cut-off parameter. The spin cut-off parameter is not known. Therefore, the experimental and the theoretical heat capacities are not directly comparable.

SUMMARY

In summary, the level densities are extracted from the experimental primary γ-ray matrix. The step structure in the level density is interpreted as pair breaking. The step structure observed experimentally should be supported by microscopic calculations. The thermodynamical properties in the ^{56}Fe isotope are studied within the canonical ensemble. The discrepancy observed between the experimental and the theoretical heat capacity may be due to the uncertainty in the value of the spin cut-off parameter in ^{56}Fe.

The method to extract level density and the γ-ray strength function has been applied earlier to several rare-earth nuclei. Here the method is extended to a lighter mass region. There have been other measurements to study ^{27,28}Si [16], whose results are submitted, and several Mo isotopes. The analysis of the Mo isotopes is in progress.

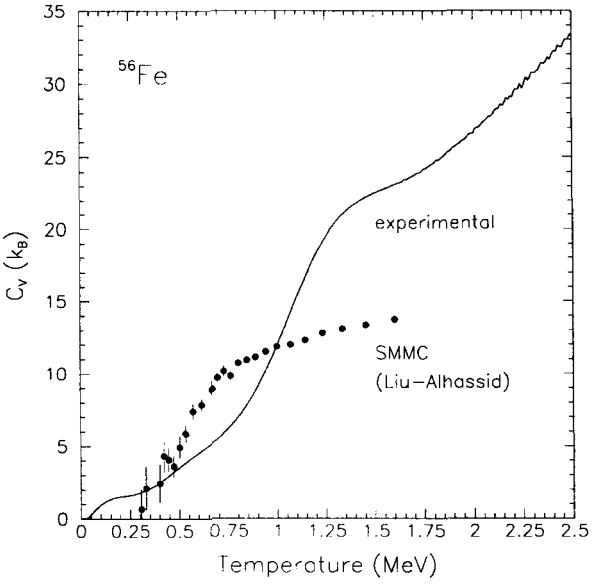

FIGURE 7. Experimental and theoretical heat capacity for ^{56}Fe.

ACKNOWLEDGMENTS

This work was performed under the grant number DE-FG02-97-ER41042 (NCSU). In addition, this work was performed under the auspices of the U.S. Department of Energy by the University of California, Lawrence Livermore National Laboratory under contract No. W-7405-ENG-48. Financial support from the Norwegian Research Council (NFR) is gratefully acknowledged.

REFERENCES

1. Schiller, A., Bergholt, L., Guttormsen, M., , Melby, E., Rekstad, J., and Siem, S., *Nucl. Instrum. Methods Phys. Res. A*, **447**, 498 (2000).
2. Melby, E., Bergholt, L., Guttormsen, M., Hjorth-Jensen, M., Ingebretsen, F., Messelt, S., Rekstad, J., Schiller, A., Siem, S., and Ødegård, S. W., *Phys. Rev. Lett.*, **83**, 3150 (1999).
3. Melby, E., Guttormsen, M., Rekstad, J., Schiller, A., Siem, S., and Voinov, A., *Phys. Rev. C*, **63**, 044309 (2001).
4. Voinov, A., Guttormsen, M., Melby, E., Rekstad, J., Schiller, A., and Siem, S., *Phys. Rev. C*, **63**, 044313 (2001).
5. Siem, S., Guttormsen, M., Ingeberg, K., Melby, E., Rekstad, J., Schiller, A., and Voinov, A., *Phys. Rev. C*, **65**, 044318 (2002).
6. Bethe, H. A., *Phys. Rev.*, **50**, 332 (1936).
7. Liu, S., and Alhassid, Y., *Phys. Rev. Lett.*, **87**, 22501 (2001).
8. Guttormsen, M., Tveter, T. S., Bergholt, L., Ingebretsen, F., and Rekstad, J., *Nucl. Instrum. Methods Phys. Res. A*, **374**, 371 (1996).
9. Guttormsen, M., Ramsøy, T., and Rekstad, J., *Nucl. Instrum. Methods Phys. Res. A*, **255**, 518 (1987).
10. Brink, D. M., Ph.D. thesis, Oxford University (1955).
11. Axel, P., *Phys. Rev.*, **126**, 671 (1962).
12. von Egidy, T., Schmidt, H., and Behkami, A., *Nucl. Phys. A*, **481**, 189 (1988).
13. Bohr, A., and Mottelson, B., *Nuclear Structure, Volume I*, World Scientific Publishing Co. Pte. Ltd., 1998.
14. Dobaczewski, J., Magierski, P., Nazarewicz, W., Satula, W., and Szymanski, Z., *Phys. Rev. C*, **63**, 24308 (2001).
15. Kittel, C., and Kroemer, H., *Thermal Physics*, Freeman, New York, 1980, p.62.
16. Guttormsen, M., Melby, E., Rekstad, J., Schiller, A., Siem, S., Loennroth, T., and Voinov, A. (2002), nucl-ex/0203013.